AIMS Materials Science, 3(3): 1281-1293.
DOI: 10.3934/matersci.2016.3.1281
Received: 30 July 2016
Accepted: 11 September 2016
Published: 19 September 2016

http://www.aimspress.com/journal/Materials

Research article

Phase evolution, microscopic analysis, optical and dielectric property evaluation of Co-doped $BaSnO_3$ by mechanical mix assisted solid state sintering method

Asima Adak (Maity) [1], Soumya Mukherjee [2,3,*], Mahua Ghosh Chaudhuri [2], and Siddhartha Mukherjee [2]

[1] Department of Electronics & Communication Engineering, Heritage Institute of Technology, Kolkata-700107, West Bengal, India
[2] Department of Metallurgical & Material Engineering, Jadavpur University, Kolkata-700032, West Bengal, India
[3] Amity School of Engineering and Technology, Amity University Kolkata Campus, Kolkata-700156, West Bengal, India

* **Correspondence:** Email: smmukherjee3@gmail.com; Tel: +919830179414.

Abstract: Cobalt (Co) doped barium stannate, i.e. $BaSn_{1-x}Co_xO_3$ with x = 0.05, 0.10 and 0.15 were prepared by mechanical mixing in agate mortar followed by sintering at 1350 °C for 2 hours. X-ray diffraction analysis (XRD) of the sample confirmed the cubic perovskite structure, crystallite size by Scherrer's formula 50 nm, 49 nm respectively and planes of orientation (110), (111), (200), (211), (220) along the major peaks. Absorption spectra obtained due to symmetric and asymmetric stretching of M–O coordinated bond formations were determined by Fourier Transform Infrared Spectroscopy (FTIR). Band gap analysis of the sintered samples evaluated using Tauc relation was obtained from UV-VIS spectral analysis while luminescence by PL spectra. Morphological analyses were carried out by SEM while EDX was done to know the presence of required elements in the samples. Particle sizes of the samples were in the range of 50–100 nm obtained by HRTEM analysis. SAED pattern was also obtained for synthesized material indicating polycrystalline nature. Higher Co doping on barium stannate leads to decrease in dielectric constant due to possible lower ionic polarization at B site of perovskite.

Keywords: nanocrystalline; barium stannate; band gap; TEM; dielectric

1. Introduction

Barium stannate is a ceramic material which has ABO_3 perovskite structure having cubic unit cell [1,2]. It behaves as an n type semiconductor with wide band gap of 3.4 eV and is thermodynamically stable at higher temperature [3]. $BaSnO_3$ has a structural similarity with the alkaline earth titanates like $BaTiO_3$ [2]. It can be used as a thermally stable capacitor and to fabricate ceramic boundary layer capacitor [2,4,5]. Barium stannate based ceramic has important application in semiconductor gas sensor device at elevated temperatures [1]. Optical properties and microstructure of the doped barium stannate exhibits many interesting and useful properties [1,6]. $BaSnO_3$ can be utilized for photoelectrochemical applications because of its band gap (3.1 eV to 3.4 eV) which is similar to important materials such as TiO_2, ZnO, $SrTiO_3$ (hydrogen photocatalyst, semiconductors) [7]. The material is observed to be thermodynamically stable at temperature up to 1273 K and higher above the mentioned one [5,7]. Inspite of higher sintering temperature required for solid state synthesis, the sample sintered above 1600 °C is observed to have porous microstructure [1,8]. $BaSnO_3$ is a dielectric material which has high dielectric constant and low loss characteristics [9].

There are limited research papers on Co doped $BaSnO_3$ having focus on the structural and optical properties of the material but synthesis routes used are quite complex and costly. In the present article Co doped barium stannate is prepared by agate mortar, pestle assisted mixing followed by sintering. The detail phase studies are carried out by XRD for phase identification. TEM confirms nanocrystalline morphology and SAED pattern ring for the nanocrystalline equimolar composite. Optical properties (band gap and fluorescence), dielectric properties of undoped and Co doped $BaSnO_3$ are measured and analysed.

2. Materials and Methods

Co doped $BaSnO_3$ with variable percentage of Co ($BaSn_{1-x}Co_xO_3$, where x = 0.05, 0.10 and 0.15) were prepared by mechanical mixing followed by sintering method. Stoichiometric amounts of BaO, SnO_2 and Co_3O_4 were mixed using agate mortar, pestle for 3 hours having pure $BaCO_3$, SnO_2 and Co_3O_4 (Merck India, Ltd) as staring precursors. Initially $BaCO_3$ was decomposed at 1250 °C to obtain pure BaO. The powders were then mixed dry (molar ratio) and sintered at 1350 °C for 2 hours in tubular furnace maintaining air as atmosphere. The sintered samples were characterized by X-ray diffractometer (Rigaku, Ultima III) using Cu source having wave length λ = 1.54 Ǻ having scan speed of 5 °/min within the scan range of 10–80°. Crystalline size was determined using Scherrer's relation $t = 0.9\lambda/\cos\theta$ where t is the crystallite size, λ is the wavelength used. The sample composition was analyzed by EDX (using ultra Dry Silicon Drift Detector from Thermo Scientific) to clarify doping of Co within barium stannate by identifying the elemental peaks of Co, Ba, Sn and O. Morphological studies were carried out by FESEM (Hitachi, S-4800). HRTEM analysis (Jeol,

2001) was done at accelerating voltage of 200 KV to confirm the morphology obtained from FESEM, in addition to interplanar fringes and the SAED pattern of the synthesized nanomaterial. For HRTEM, sample was prepared by dispersing in ethanol medium with a sonicator for 1 hour and then dropped it over the carbon coated copper grid for analysis. Stretching and vibration of absorption bands were characterized by FTIR (FTIR Shimadza, IR-21 prestige) within scan range of 5000–400 cm^{-1}. For FTIR analysis, sample was mixed with KBr and pellets were formed in steel die having diameter of 10 mm under pressure of 6 tonne/cm^2. For UV-VIS study, sample was sonicated in deionized water for about 1 hour till clear solution was observed and scanning of spectra was carried in the range of 150−750 nm. Band gap were evaluated using Tauc relation from spectra, from UV-VIS spectrophotometer (Perkin Elmer, Lambda 35). For spectrophotometer emission study, sample preparation was similar to UV-VIS analysis where the prepared solution was put into quartz cuvette for spectroscopic study. Emission studies were also carried out in Spectrofluorometer (SL-174, Elico) having 150W Xe laser source and PMT. Pellets of undoped sample and two Co doped samples were prepared by pressurizing the powder samples into circular discs of thickness 1 mm or 2 mm and diameter 12 mm by applying a pressure of 30 kg/cm^2 for 2 min in a hydraulic press. Both surfaces of the pellets were metalized by silver pasting. Dielectric properties were measured using 4294A Precision Impedance Analyzer (Agilent).

3. Results and Discussion

3.1. Phase Determination by XRD

X-ray diffraction pattern of Co doped barium stannate sintered at 1350 °C for 2 hours with different doping percentage is shown in Figure 1(a–c). It has been observed that all the identifed peaks are indexed to cubic perovskite structure. Crystalline phase nucleation, growth occurs along (110), (111), (200), (211), (220) and (310) directional planes of minimum energy facets and peak position matches well with ICDD-JCPDS, PDF data (Card No. #150780) [10]. Crystallite size of the powder sample is determined by Debye-Scherrer formula $D = 0.9\lambda/\beta\cos\theta$ where D is the crystallite size, λ is the wavelength of the X-rays used, β is the broadening of diffraction line measured at the half of its maximum intensity in radians and θ is the angle of diffraction [11]. The variation of crystallite size with the different concentration of Co doping $BaSnO_3$ is very small while peak position of maximum intensity is also noted to have varied negligibly with higher doping concentration [12]. Crystallite size for undoped sample is noted to be around 50 nm while high intensity planes being about $2\theta = 30.68°$ [25]. Respective position of main peak 2θ position for 5%, 10%, 15% Co doping are 30.74, 30.75 and 30.77 respectively. The average crystallite size is noted to be around 49 nm and matches well with corresponding previous articles [4]. Thus strain have been introduced which increases with doping due to increment in variation of angle differences (higher doping concentrations) and differences of atomic radii between Sn^{4+} and Co ion. Atomic radius of Sn^{4+} is 83 pm (octahedral coordination) while that of Co ion is 75 pm. This Co ion is of high spin state due to transition or jump of electron from one state to another.

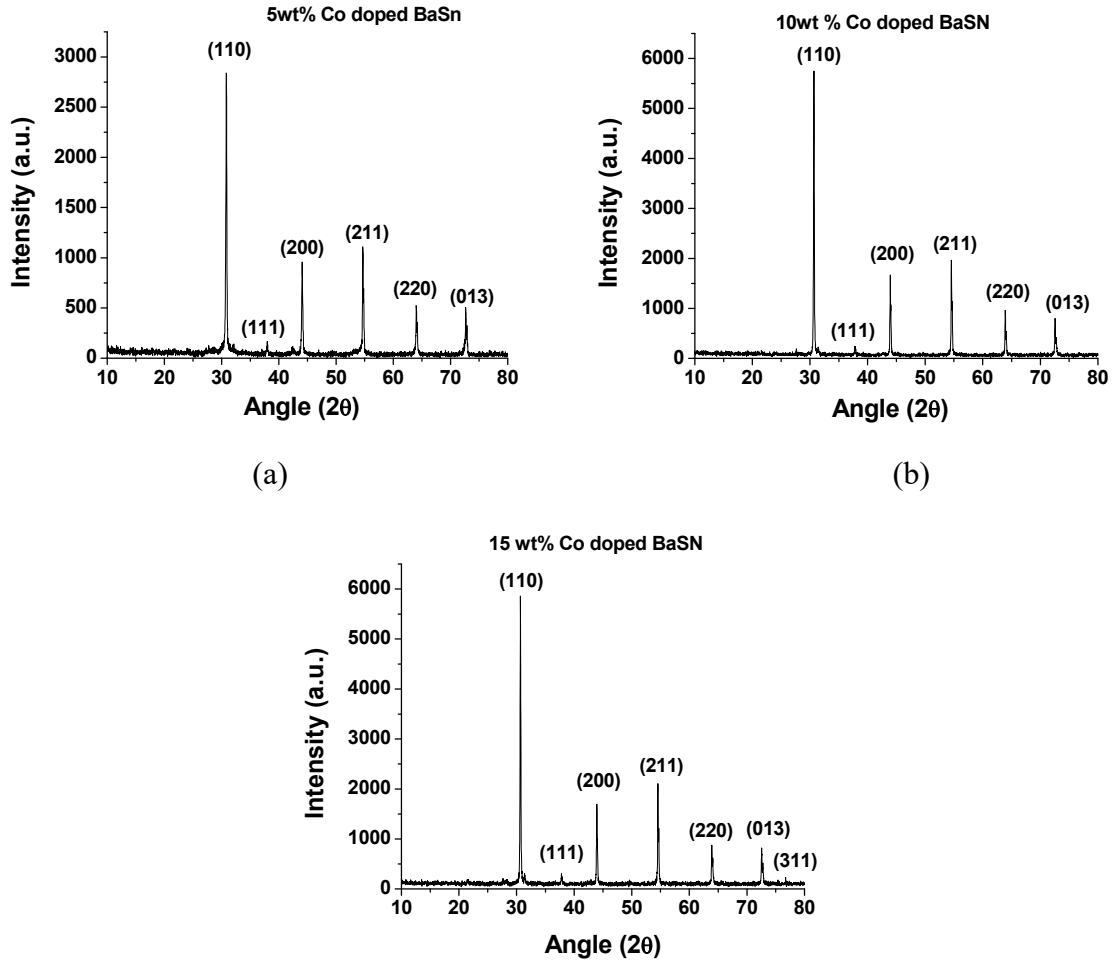

Figure 1. X-Ray diffraction pattern of (a) 5% Co doped and (b) 10% Co doped and (c) 15% Co doped $BaSnO_3$ powder sample.

3.2. FTIR Spectroscopy Analysis

FTIR absorption spectra of the sample exhibits characteristic peaks due to scan in the range between 400 cm^{-1} to 5000 cm^{-1} for Co doped barium stannate with different concentration as shown in Figure 2(a–c). It has been observed in our previous experimental research that Sn–O vibration is within 450–600 cm^{-1}. For undoped sample dominant [SnO_6] octahedron structure with prominent stretching is noted to be about 658 cm^{-1} [25]. In the present article, for Co doped samples, Sn–O stretching vibration is observed at 432 cm^{-1} and 641 cm^{-1} for lower doping concentration [13]. This bond is slightly found to increase with higher concentration of doping. Thus, dominant peak for all three dopants at about 641 cm^{-1} or 654 cm^{-1} represents [SnO_6] octahedron structure which has symmetrical stretching vibration [12]. The small peak at 1031 cm^{-1} and dominant peak at 1421 cm^{-1} for all three compositions attributes the C–O stretching vibration [12]. Moreover the samples have shown the characteristics band of $BaCO_3$ due to presence of atmospheric carbonates and minute traces of unconverted carbonates [6,14].

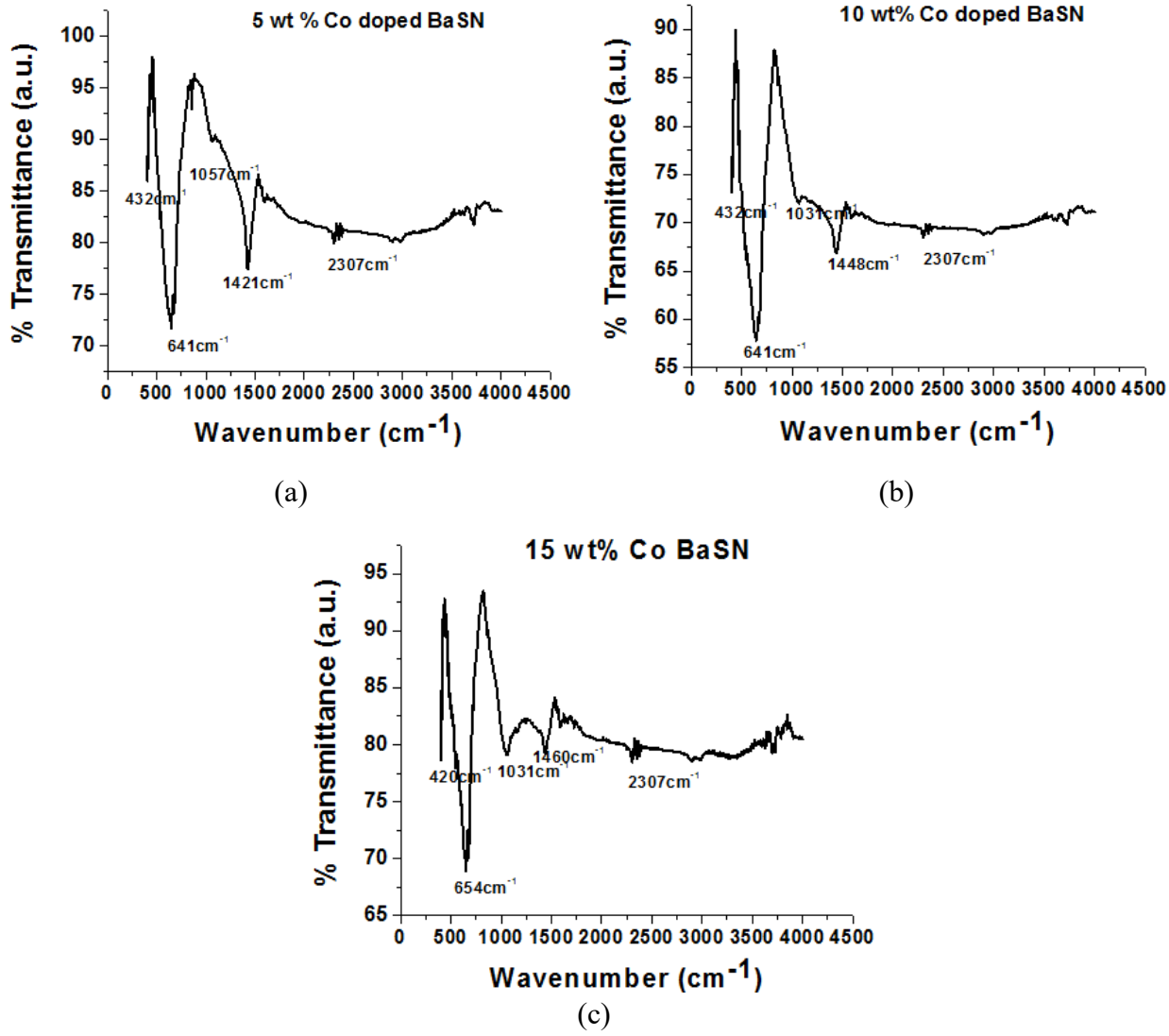

Figure 2. Fourier Transform Infrared spectrum of (a) 5% Co doped $BaSnO_3$ (b) 10% Co doped $BaSnO_3$ and (c) 15% Co doped $BaSnO_3$.

3.3. UV-VIS Spectroscopy & PL Analysis

For UV/VIS spectral analysis, absorption spectra of the sample is measured in the range between 200 nm to 700 nm for Co doped barium stannates as shown in the Figure 3(a–c). Powder samples are dispersed in deionized water solvent by sonication for preparing the sample solution. From Figure 3, it has been shown that there are prominent absorption peak in the range between 200 nm to 300 nm which exhibit absorption in UV region than visible region [15]. Similar scan is carried for undoped samples having absorption peaks in the same range of wavelength [26]. Some previous research article revealed that band gap is in the range of 2 eV to 3.4 eV for undoped sample [16]. From Figure 4(a–e), it has been shown that for 5% Co doped $BaSnO_3$, band gap energy of indirect transition, direct transition are 3.17 eV, 3.28 eV respectively and observed to be closely in correspondence with previous findings. Similarly, for 10%, 15% Co doping indirect and direct

transitions are about 2.76 eV, 3 eV and 2.4 eV, 3.134 eV respectively. It is found that Band gap energy of Co doped $BaSnO_3$ decreases with increase in Co concentration than undoped barium stannate [12,14]. For undoped sample, indirect and direct transition is found to be about 2.78 eV, 3.14 eV respectively. That causes shifting of absorption edge towards higher energy with increase in free electron concentration [17,18]. Tauc plot for determination of band gap is also noted for ZnO synthesizd by PECVD, sol-gel process [19,20]. Such change in band gap is due to generation of defect energy level within the band structure of the material system. Figure 5 shows the study of the photoluminescence (PL) spectrums measured for undoped and Co doped barium stannate sintered at 1350 °C for 2 hours with different compositions. A room temperature PL spectrum of the perovskite (Figure 5a–c) is obtained after excitation at constant wavelength of 250 nm with emission peak around 371 nm for all three dopant concentrations. Strong emission is observed at 371 nm in the UV region. So nanocrystalline $BaSnO_3$ is a photoluminescent material and a slight shift of intense emissions of the PL spectrums is observed due to increase of Co concentration.

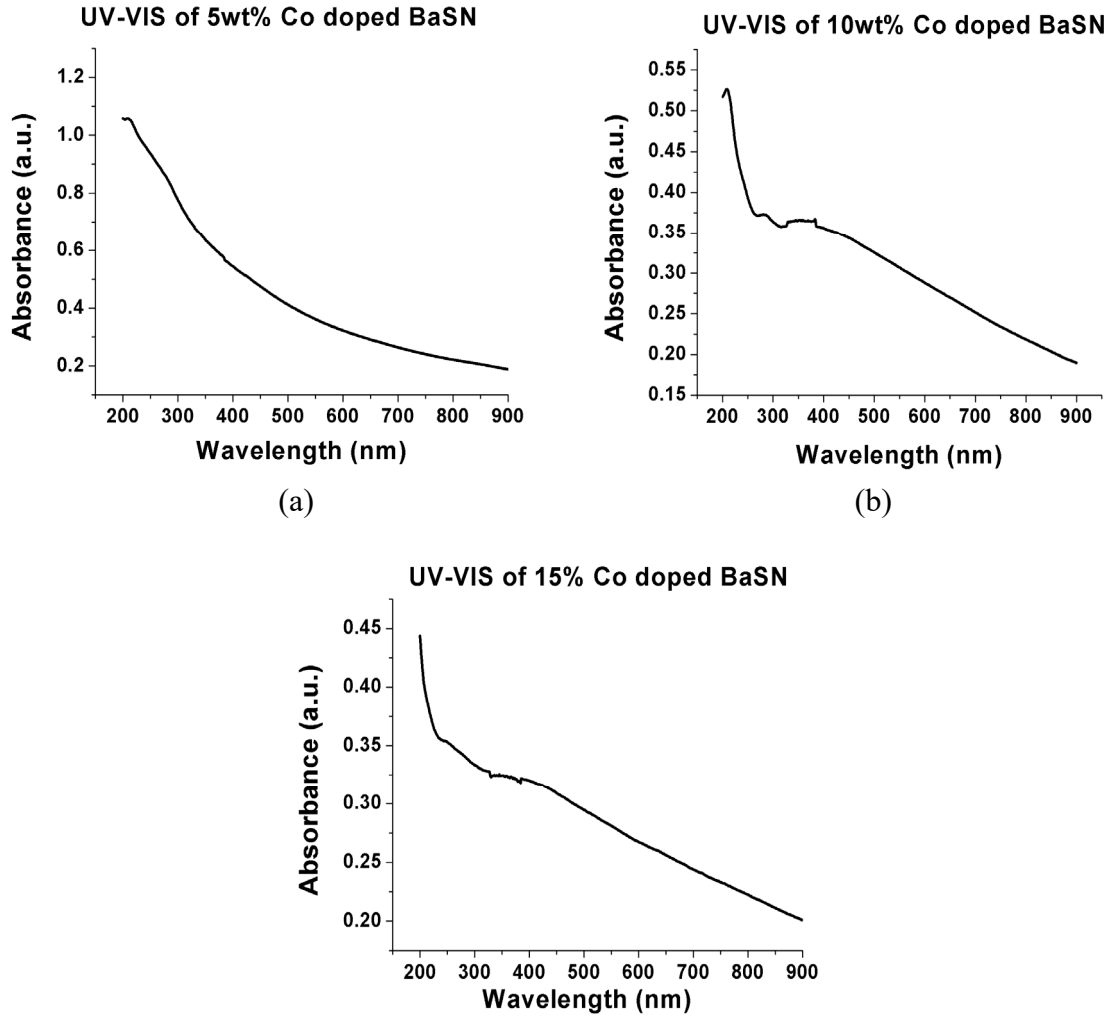

Figure 3. Absorption spectra of (a) 5% Co doped $BaSnO_3$ (b) 10 % Co doped $BaSnO_3$ (c) 15% Co doped $BaSnO_3$ measured in the range from 200 nm to 700 nm.

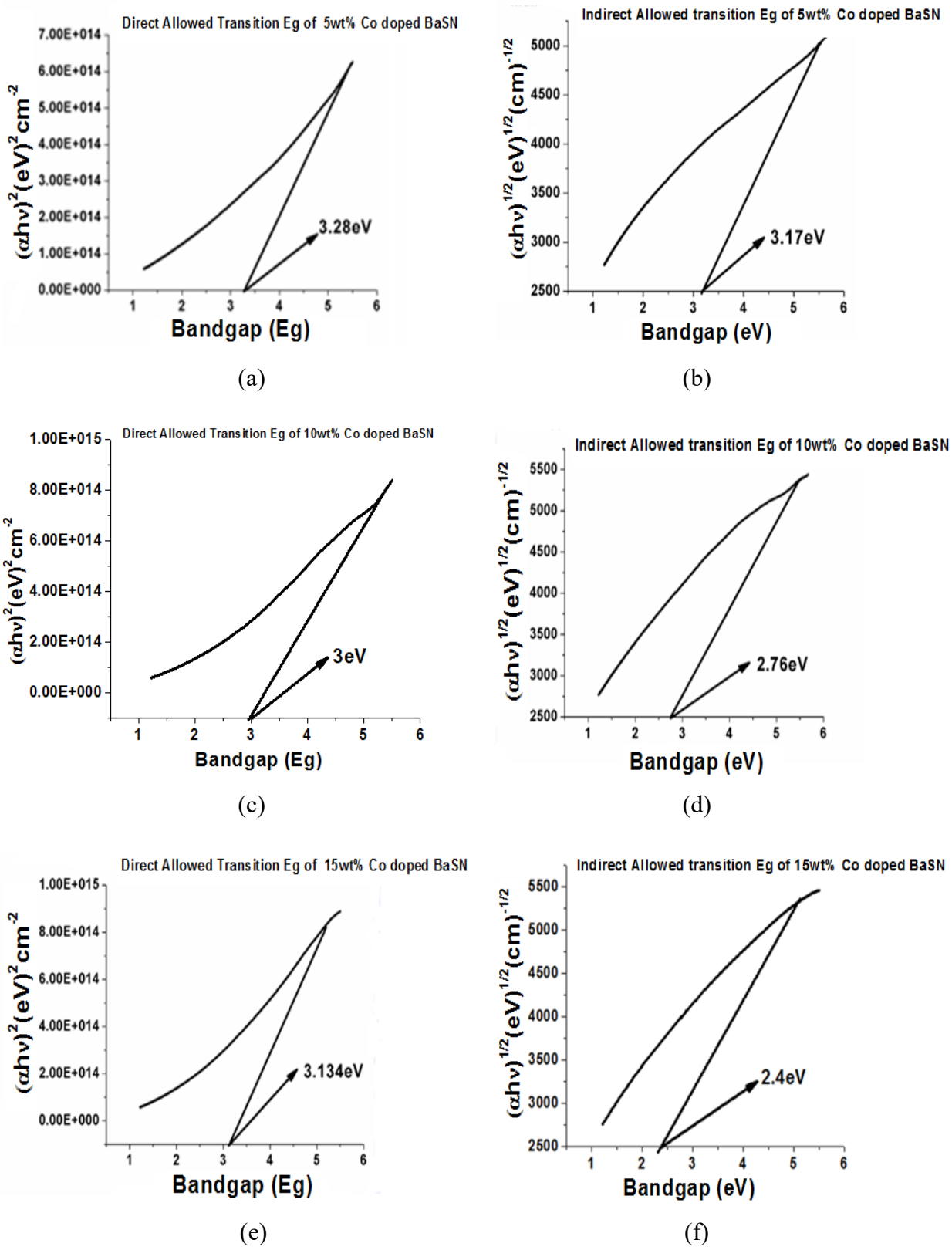

Figure 4. Plot of $(\alpha h\nu)^2$ and $(\alpha h\nu)^{1/2}$ of (a), (b) 5% Co (c), (d) 10% Co and (e), (f) 15% **Co** doped $BaSnO_3$ nanoparticles for direct and indirect transition.

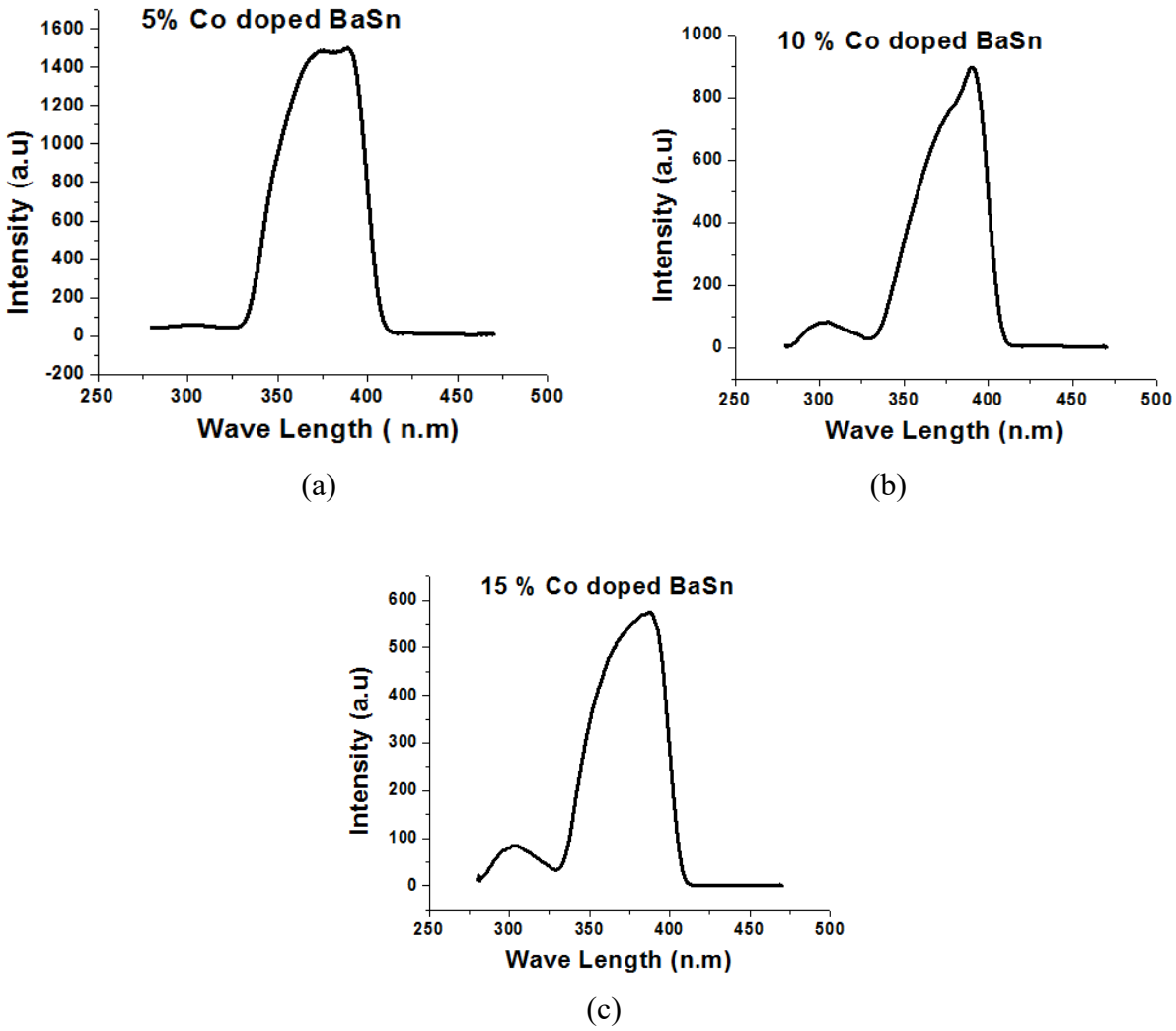

Figure 5. Photoluminescence spectrums of (a) 5% Co (b) 10% Co and (c) 15% Co doped $BaSnO_3$ powder sample.

3.4. Morphological Studies

3.4.1. Microstructure and Morphological Studies by SEM and Elemental Analysis by EDX

SEM micrographs of Co doped barium stannate $BaSn_{1-x}Co_xO_3$ with x = 0.05, 0.10 and 0.15 are shown in Figure 6(a–c). Micrograph of all the samples shows massive agglomerations with interconnection among particles. All the samples of Co doped BaSn with different composition exhibits interconnected agglomerates with no preferred directional growth. Some interconnected pores are also noted amongst the agglomerate structure where the individual grains are having cubical to spherical morphology. The average grain size for the samples with x = 0.05 and x = 0.1 is less than a 1 μm [18]. Average grain size for the samples with x = 0.15 is almost 1 μm which indicate the variation of the grain size with different compositions of Co doped $BaSnO_3$ which is found to be small. The Figure 6d shows the results of EDX spectra for elemental analysis of

synthesized material. The results confirmed the presence of the elements (Ba, Sn, Co and O) in the calculated ratio responsible for the formation of required nano-crystalline perovskite compound.

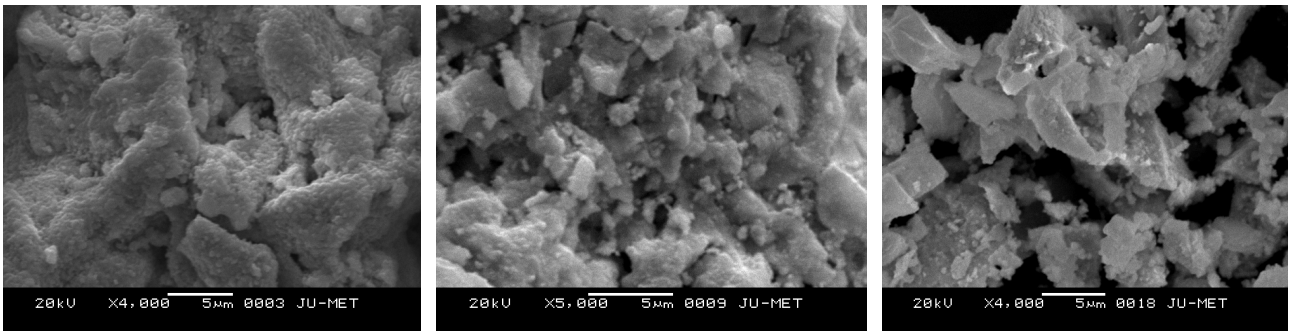

(a) (b) (c)

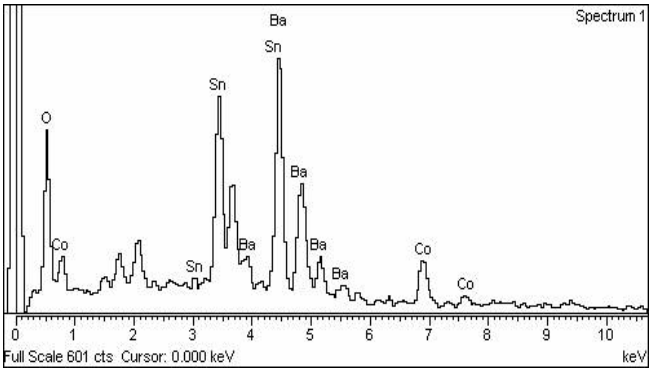

(d)

Figure 6. SEM images of $BaSn_{1-x}Co_xO_3$ for (a) x = 0.05 (b) x = 0.10 (c) x = 0.15 and (d) EDS spectra of $BaSn_{1-x}Co_xO_3$ exhibiting spectra of elements present within the material.

3.4.2. Microstructure of HRTEM Morphology and SAED Pattern

HRTEM image (Figure 7a–d) shows the morphology and SAED pattern ring for the nanocrystalline undoped and Co doped barium stannate after heat treatment at 1350 °C for 2 hours. The morphological nature obtained from HRTEM analysis exhibits quasi-spherical and polygonal type nanopaticles. The mean particle sizes of 5 percent Co doped are about 50 nm [21,22,23]. It is observed that particle size of Co doped $BaSnO_3$ remain unchanged or slight changes occur with increasing dopants on barium stannate. SAED (Selected Area Electron Diffraction) arises from diffraction of interplanar spacings present in the material system follows principle of reciprocal lattice. The SAED pattern exhibits diffraction patterns of interplanar fringes, corresponding to polycrystalline nature of the synthesized nanoparticles. In undoped samples SAED pattern index has shown the main part of diffracted spots, information belongs to the $BaSnO_3$ crystalline structure (5 rings) [24]. As doping increases, there is only one diffraction ring appears. The result from SAED justifies the findings from XRD studies.

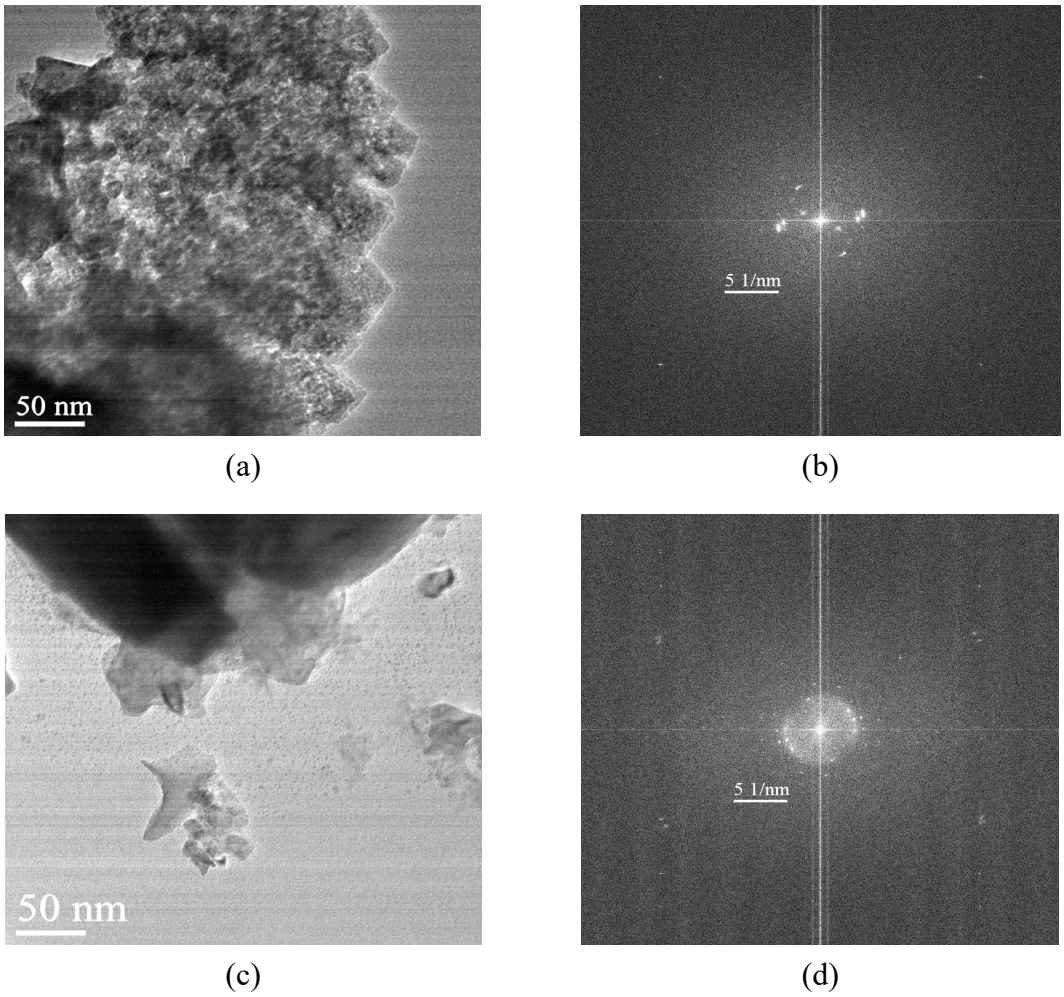

Figure 7. HRTEM morphology and SAED pattern of (a), (b) 5% Co and (c), (d) 10% Co doped $BaSnO_3$ powder sample.

3.5. Dielectric Properties

The frequency dependence of capacitance and relative permitivity of Co doped barium stannate with different composition are shown in the Figure 8(a–b). Capacitance is found to decrease till 40000 Hz and becomes constant with increasing composition of Co doped barium stannate. It is observed that permittivity also decreases with increasing composition of doped $BaSnO_3$ [9]. The decrease in capacitance, permittivity with increase in frequency is due to space charge polarization. Such phenomenon arises due to inertia of effective masses of electron cloud leading to frequency lag with applied bias. Such behavior of dielectric constant with frequency is found to be consistent with previous reports on other material like Co, Ni doped Bismuth ferrite [26]. The dielectric constant observed for 10% Co doped barium stannate is around 80 while that of 15% Co doped sample is around 27. Due to doping of higher percentage of Cobalt at Sn^{4+} sites, partial replacements at B site occurs. From electronic configuration of Co^{2+} ions it is evident that there will 5 Bohr magneton spin magnetic moment. Since the magnetic character increases polarizability will decrease and hence

dielectric constant falls sharply at 15% Co doping. Thus, the present percentage indicates a sharp change in electronic behavior of the material due to doping.

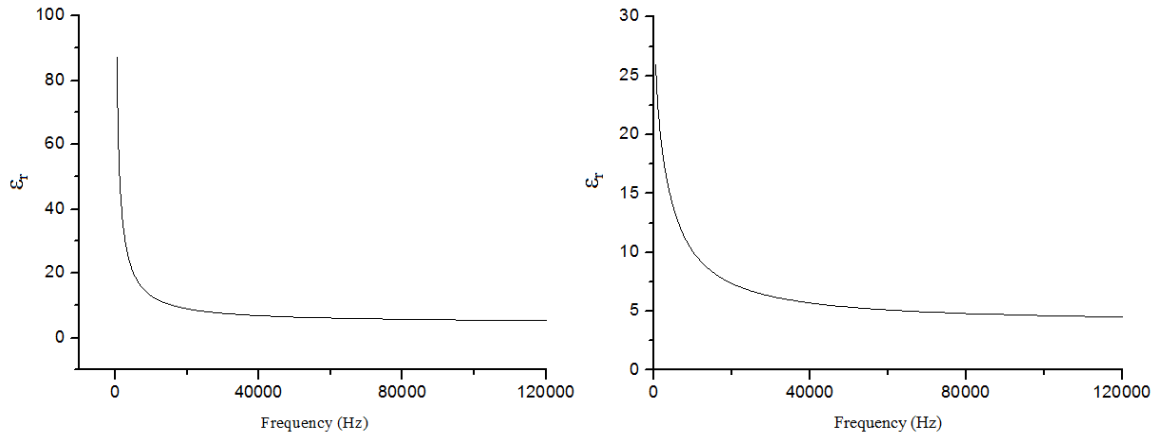

(a) (b)

Figure 8. Response of relative permittivity with frequency of (a) 10 % Co and (b) 15% Co doped $BaSnO_3$ powder sample.

4. Conclusions

Cobalt (Co) doped barium stannate, i.e. $BaSn_{1-x}Co_xO_3$ with x = 0.05, 0.10 and 0.15 are prepared by mechanical mixing by agate mortar followed by sintering at 1350 °C for 2 hours. XRD reveals cubic perovskite type of structure having crystallite size about the range of 49 nm. Crystallite size variations with different percentile of Co doped $BaSnO_3$ is very small. Sn–O stretching vibration, C–O stretching vibration bands are noted from the FTIR spectral analysis. Sn–O stretching vibration bond decreased slightly with increase in dopant concentrations. All three compositions have same C–O stretching vibration bond. From UV-VIS analysis, it have been reflected that samples absorb mostly in the UV region having band gap values near to semiconductor material range. PL emission is about 371 nm which is close to visible range. Band gap energy decreases with increasing composition. Morphological studies by SEM revealed nature of granular formations and it has been observed that grain size is less than 1 μm. EDX analysis has confirmed the presence of elements responsible for the cobalt doped barium stannate formations. HRTEM analysis exhibits quasi-spherical and polygonal type nanopaticles while SAED pattern exhibits diffraction rings which correspond to polycrystalline nature of the nanoparticles. As doping increases, there is appearance of only one diffraction ring which decreases than pure sample (5 rings). From dielectric property analysis it has been shown that Capacitance is found to decrease till 40000 Hz and becomes constant with increasing composition of Co doped barium stannate.

Acknowledgements

We are greatly indebted to Department of Metallurgical & Materials Engineering, JU, Kolkata, India, for giving us the opportunity to take up this interesting project work. It is our privilege to

convey our heartiest thanks to research scholars and Technical Staff for carrying out the characterization.

Conflict of Interest

All authors declare no conflict of interest.

References

1. Singh P, Sebastian PC, Kumar D, et al. (2007) Correlation of microstructure and electrical conduction behaviour with defect structure of niobium doped barium stannate. *J Alloy Compd* 437: 34–38.
2. Upadhyay S, Parkash O, Kumar D (2001) Solubility of lanthanum, nickel and chromium in barium stannate. *Mater Lett* 49: 251–255.
3. Doroftei C, Popa DP, Iacomi F (2012) Study of the influence of nickel ions substitutes in barium stannates used as humidity resistive sensors. *Sensor Actuat A-Phys* 173: 24–29.
4. Lu WS, Schmidt H (2008) Lyothermal synthesis of nanocrystalline $BaSnO_3$ powders. *Ceram Inter* 34: 645–649.
5. Kocemba I, Jedrzejewska WM, Szychowska A, et al. (2007) The properties of barium stannate and aluminum oxide-based gas sensor The role of Al_2O_3 in this system. *Sensor Actuat B-Chem* 121: 401–405.
6. Alves CFM, Soraia CS, Limaa HSH, et al. (2009) Influence of the modifier on the short and long range disorder of stannate perovskites. *J Alloy Compd* 476: 507–512.
7. Bouhemadou A, Haddadi K (2010) Structural, elastic, electronic and thermal properties of the cubic perovskite-type $BaSnO_3$. *Solid State Sci* 12: 630–636.
8. Wei XY, Feng YJ, Hang LM, et al. (2005) Abnormal *C–V* curve and clockwise hysteresis loop in ferroelectric barium stannate titanate ceramics. *Mater Sci Eng B-Adv* 120: 64–67.
9. Singh S, Singh P, Parkash O, et al. (2010) Structural and relaxor behavior of $(Ba_{1-x}La_x)(Ti_{0.85}Sn_{0.15})O_3$ ceramics obtained by solid state reaction. *J Alloy Compd* 493: 522–528.
10. Omeiri S, Hadjarab B, Bouguelia A, et al. (2010) Electrical, optical and photoelectrochemical properties of BaSnO applications to hydrogen evolution. *J Alloy Compd* 505: 592–597.
11. Cullity DB (1956) Elements of X-ray diffraction, Addison-wesley Publishing Company, INC. Reading, Masachusetts.
12. James KK, Aravind A, Jayaraj MK (2013) Structural, optical and magnetic properties of Fe-doped bariumstannate thin films grown by PLD. *Appl Surf Sci* 282: 121–125.
13. Köferstein R, Abicht HP, Woltersdorf J, et al. (2006) Phase evolution of a barium tin 1,2-ethanediolato complex to barium stannate during thermal decomposition. *Thermochim Acta* 441: 176–183.
14. Charles MW, Nick H, Gregory ES (1989) Physical Properties of Semiconductors, Prentice-Hall, Englewood Cliffs, New Jersey Edition.

15. Vidya S, Rejith PP, Annamma J, et al. (2011) Electrical, optical and vibrational characteristics of nano structured yttrium barium stannous oxide synthesized through a modified combustion method. *Mater Res Bull* 46: 1723–1728.
16. Köfersteina R, Yakuphanoglub F (2010) Semiconducting properties of Ge-doped $BaSnO_3$ ceramic. *J Alloy Compd* 506: 678–682.
17. Maity A, Mukherjee S, Chaudhuri MG, et al. (2015) Phase evaluation, microscopy and band gap of Fe-doped nanocrystalline $BaSnO_3$ by solid state sintering assisted with agate mortar activation. *Int J Current Eng Tech* 5: 3829–3834.
18. Moss TS (1954) Pceedings of the Physical Society, London, Section B, 67: 775.
19. Arif B (2015) Determination of optical constants of ZnO growth by PECVD Method. *J Mater Electron Dev* 1: 28–32.
20. Aksoy S, Ruzgar S (2015) Effect of Nitrogen on optical properties of ZnO film deposited by sol gel method. *J Mater Electron Dev* 1: 33–37.
21. Udawatte CP, Kakihana M, Yoshimura M (1998) Preparation of pure perovskite-type $BaSnO_3$ powders by the polymerized complex method at reduced temperature. *Solid State Ionics* 108: 23–30.
22. Du FT, Cui B, Cheng HL, et al. (2009) Synthesis, characterization, and dielectric properties of $Ba(Ti_{1-x}Sn_x)O_3$ nanopowders and ceramics. *Mater Res Bull* 44: 1930–1934.
23. Li HB, Tang WY, Luo JL, et al. (2010) Fabrication of porous $BaSnO_3$ hollow architectures using $BaCO_3$@SnO_2 core-shell nanorods as precursors. *Appl Surf Sci* 257: 197–202.
24. Cerda J, Arbiol J, Diaz R, et al. (2002) Synthesis of perovskite-type $BaSnO_3$ particles obtained by a new simple wet chemical route based on a sol-gel process. *Mater Lett* 56: 131–136.
25. Maity A, Mukherjee S, Chaudhuri MG, et al. (2015) Phase evaluation of pure nanocrystalline barium stannate by two different milling activations. *Inter Ceram* 64: 276–280.
26. Mukherjee S, Sarkar K, Mukherjee S (2015) Effect of Nickel and Cobalt doping on nano Bismuth Ferrite prepared by the chemical route. *Inter Ceram* 64: 38–43.

AIMS Press